# Structural and cation distribution analysis of Nickel-Copper/Nickel-Magnesium substituted Lithium Ferrites

**D. Parajuli[1,*], K. Samatha[2]**

[1]*Research Center for Applied Sc. and Tech., Tribhuvan University, Kirtipur, Kathmandu, Nepal*
[2]*Dept. of Physics, College of Sc. and Tech., Andhra University, Visakhapatnam, India*

*Corresponding author. Email: deepenparaj@gmail.com

**Abstract**

*Lithium ferrite ($Li_{0.5}Fe_{2.5}O_4$) is a promising material due to its importance in construction and engineering. It can be crystallized in the spinel crystal structure, $AB_2O_4$, where "A" and "B" depict lattice sites named as tetrahedral and octahedral supported by oxygen ions, respectively. The XRD peaks are matched well with the JCPDS card (no. 38-0259) indicating a spinel cubic crystal structure with the space group of* Fd3m *except for for extra peak 211 in the basic lithium ferrite as an indication of the mild phase transformation from the Fd3m space group to the $P4_132$ space group. The present basic Li-ferrite sample contains a mild secondary hematite phase too apart from the major spinel crystal phase. The cation distribution is also tested in this work which is important for further investigation of magnetic and dielectric properties of the ferrites. These ferrites are widely used in microwave, magnetic as well as electric energy storage devices.*

## 1 Introduction

Lithium ferrites are considered to be one of the most versatile ferrites as it covers a large number of applications. Lithium ferrites are frequently used in information storage, switching devices, and phase shifters because of their excellent rectangular hysteresis loop characteristics [1, 2]. It has a relatively high curie temperature of about 640ºC, which ensures its applicability over a wide range of technically useful temperatures. At room temperature, lithium ferrite has permeability and saturation magnetization higher than those for Yttrium iron garnet. It has a low cost when compared to the garnets [3]. The nickel-rich Lithium ferrites

are also extensively used for Lithium-ion batteries [4], [5]. Lithium ferrite (Li0. 5Fe2. 5O4) is a promising material due to its importance in construction and engineering [6]. It can be crystallized in the spinel crystal structure, AB2O4, where "A" and "B" depict lattice sites named as tetrahedral and octahedral supported by oxygen ions, respectively [7]. Lithium and Magnesium ferrites are potential materials for applications from low frequency to microwave frequencies [8–10]. The Li and Mg Ferrites, with their high resistivity and low eddy current losses, are useful materials for applications at microwave frequencies. They exhibit rectangular hysteresis loops, which makes them suitable for magnetic information storage devices. Moreover, these materials are cost-effective with easy preparation techniques, and excellent performance over a wide range of temperatures compared to garnets that have similar applications. This has attracted scientists and technologists for widespread development of materials in different devices. Ferrites are mostly, as prepared as ceramic materials by conventional methods [4, 11, 12]. The study of structural properties with XRD is related to the crystal structure, cation distribution, and surface microstructures which are composed of pores, grains, and grain boundaries.

Thus, structural studies are essential for understanding the variations of magnetic and electrical properties as well as developing suitable materials for microwave applications. Since the observed variations in saturation magnetization (to be discussed in the next paper) would also provide valuable information about the distribution of cations in $Li_{0.5-x}Ni_xCu_xFe_{2.5x}O_4$ (LNC) and $Li_{0.5-x}Ni_xCu_xFe_{2.5}xO_4$ (LNM) (x=0.00, 0.05, 0.10, 0.15, 0.20, 0.25) ferrite systems, the discussions involved in arriving at the cation distributions can be used to verify and confirm the distributions are presented in this paper.

## 2 Materials preparation and characterization

The starting materials were reagent-grade lithium oxide, nickel oxide, copper oxide, magnesium ox-

ide, and iron oxide powders which were mixed in appropriate stoichiometric ratio and ground for 12 hours using agate mortar and pestle in the presence of methanol to improve homogeneity. The resulting mixture was air-dried and then pre-sintered in the air for 8 hours at 750°C. The pre-sintered ferrite was again ground for 4 hours in the presence of methanol and again dried in air at room temperature. The prepared samples were designated as LNC series: $Li_{0.5-x}Ni_xCu_xFe_{2.5x}O_4$, (x=0.00, 0.05, 0.10, 0.15, 0.20, 0.25) and LNM series: $Li_{0.5-x}Ni_xMg_xFe_{2.5x}O_4$, (x=0.00, 0.05, 0.10, 0.15, 0.20, 0.25) with LNC and LNM respectively.

The structural characterization of the samples Li0.5Fe2.5O4 were done with X ray diffractometer (Rigaku).

## 3 Results

### 3.1 X-ray diffraction studies

Typical X-ray powder diffraction patterns of $Li_{0.5}Fe_{2.5}O_4$ (basic Lithium ferrite), $Li_{0.5-x}Ni_xCux$ $Fe_{2.5x}O_4$ (LNC x=0.10) and $Li_{0.5-x}Ni_xMg_xFe_{2.5x}O_4$ (LNM x=0.10) are shown in Figures 1, 2 and 3 respectively. The XRD peaks 210, 211, 220, 310, 311, 321, 400, 421, 422, 511, 440 are matched well with JCPDS card (no. 38-0259). The patterns are indexed with all the planes indicative of spinel cubic crystal structure with the space group of *Fd3m*. However, the basic lithium ferrite shows some extra peaks with the hkl values of 211 which is indicative of a mild phase transformation from the Fd3m space group to $P4_132$ space group. From the X-ray diffraction studies, the lattice constant of the basic composition $Li_{0.5}Fe_{2.5}O_4$ sintered under different conditions has been determined in this paper. This study reveals that the lattice constant does not change with the sintering conditions as is to be expected. The measured value of the lattice constant along with the values reported in the literature for the above composition are given in table1 for comparison.

Table 1: Lattice constant values in Å for $Li_{0.5}Fe_{2.5}O_4$.

| Present Study | From the Literature |
|:---:|:---:|
| $8.287 \pm 0.005$ | 8.328 [13], 8.298 [14], 8.301 [15] |

As is evident from the data that the values reported in the literature differ slightly from each other since the origin and method of preparation of the sample under test is different for different cases [16]. However, the observed value in the present study lies well within the reported range of lat-

tice parameter values. This kind of transformation is more in the basic lithium ferrite, and quite less in substituted lithium ferrites. Particularly, when the concentration of the Ni-Cu or Ni-Mg cations is substituted in place of Li-Fe ions this extra phase for transformation gradually disappears and finally for concentrations x=0.20 onwards the patterns are clearly indicative of spinel crystal structures with only Fd3m space group. A marked reduction in the intensity of 210 peak and complete elimination of 211 peak in the XRD patterns of substituted samples can be clearly seen in comparison to the XRD pattern of the basic lithium ferrite.

Similarly, it is noticed that apart from the presence of 310 peak, the intensities of 422 and 311 peaks appear more than what the spinel crystal structure normally produces. In this case too, the differences in normal intensities of 422, 311 and 310 gradually decrease when the concentration of the substituted Ni-Cu or Ni-Mg cations increases. Hence, we have made an attempt to index these extra peak intensities to the 132, 110 and 121 peaks represented by hematite (antiferromagnetic - $Fe_2O_3$) crystal structure and they are well matched.

Thus, it can be said from the above that the present basic Li-ferrite sample contains a mild secondary hematite phase too apart from the major spinel crystal phase. Here too, a marked reduction in the magnitude of hematite phase in the XRD patterns of substituted samples is observed when the concentration of the substituted Ni-Cu or Ni-Mg cations increases.

## 3.2 Cation distribution analysis

### 3.2.1 Observed lattice parameter

The main reflection planes of the spinel structure of ferrites are identified in the X-ray diffraction patterns of the present samples as (220, 311, 400, 422, 511 and 440). Using all these major peaks of the spinel structure, experimental lattice parameters were estimated for all the samples. In order to minimize the error in estimations, the obtained lattice parameters were plotted versus the Nelson –Riley error function [17].

The plots are straight lines with increasing trends. The observed lattice parameter can be obtained by extrapolating the lines to =90º, where all errors vanish. The estimated values of the experimental lattice parameter "$a_{\mathrm{exp}}$" as a function of composition (x) for both the LNC and LNM ferrite systems are presented in Figure 4. The lattice constant has been observed to increase with concentration (x) in both the series. Further, it is observed to

increase steeply from x = 0.10 onwards till x=0.20 in all the substituted samples.

The introduction of Ni2+ and Cu2+ ions in LNC series, and Ni2+ and Mg2+ ions in LNM series into Li0.5Fe2.5O4 can cause a small shift in the lithium ferrite peaks. This shift is indicative of the change in lattice constant. Larger size ions, Cu2+ ions in LNC series and Mg2+ ions in LNM series cause the spinel lattice of the lithium ferrite to expand. This increment of the lattice parameter could be explained on the basis of ionic radii, where the radius of Ni2+ ion (0.069 nm) is smaller than that of Li+ (0.073 nm) and radius of Cu2+ion (0.073nm) is larger than of Fe3+ (0.0645 nm) ions. In LNM series, the Ni2+ ions successively replace the Li+ and the Mg2+ (0.072 nm) ions replace Fe3+ (0.0645 nm) ions.

This introduction of larger size ions, i.e., Cu2+ and Mg2+, is likely to induce uniform strain in the lattice, as the material is elastically deformed. This effect causes the lattice plane spacing to change and the diffraction peaks to shift to a lower 2 position [18, 19]. The unit cell expands to accumulate the larger ion, so it is expected to increase the lattice parameter. The uniform increase in lattice constant with Ni-Cu and Ni-Mg substitution indicates that lattice expands without disturbing the symmetry of lattice [20]. A similar variation has also been reported by Ravinder et al. [21].

### 3.2.2 Theoretical lattice parameter

In order to match the trend of the observed lattice constants with theoretical ones in both LNC and LNM series, a careful selection of cations among the tetrahedral and octahedral sites was assigned. This has been a common practice in assigning cation distributions [22] because the cations take different values in their dimensions depending up on their occupation in particular lattice site and its corresponding coordination. For example, the ionic radius of Cu2+ ions in tetrahedral (4-fold) coordination is equal to 0.57 Å and in octahedral (6-fold) coordination its size becomes 0.73 Å. This difference in size due to its occupation in a particular site would also naturally affect the lattice constant. In the light of this information, an attempt was made in the present work to match the lattice constant by carefully assigning the cations in A- and B-sites. However, since such a distribution should also match with the cation distribution to be assigned when the theoretical and experimental magnetic moments (to be discussed in the next paper) are compared, we have put up a concentrated effort in making these assignments by synchronizing all the experimentations on these samples.
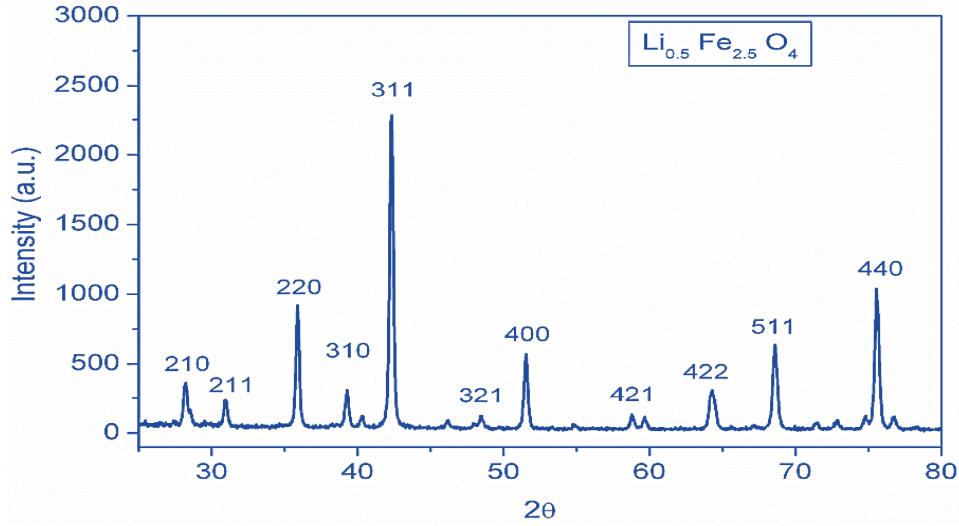
Figure 1: Typical X-ray diffraction pattern of lithium ferrite.
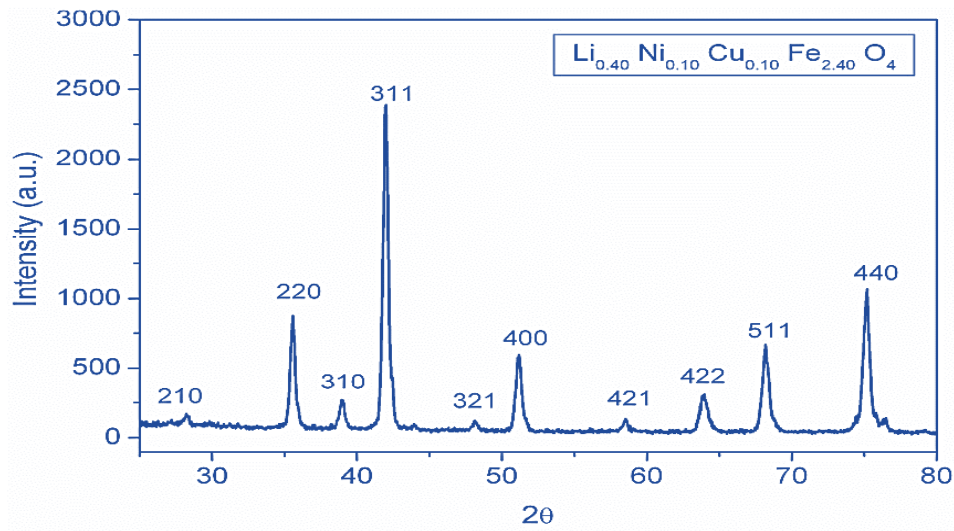


Figure 2: Typical X-ray diffraction patterns of Ni-Cu substituted (LNC, x=0.10) and Ni-Mg substituted (LNM, x=0.10) ferrite samples.

Theoretical lattice constant in general is calculated using the following relation [23].

$$a_{\text{th}} = \frac{8}{3\sqrt{3}} \left\{ (r_A + R_o) + \sqrt{3}\,(r_B + R_o) \right\} \tag{1}$$

Here $r_A$ and $r_B$ are the mean radii of the tetrahedral and octahedral sites and $R_o$ is the radius of oxygen ion.

In LNC series,

$$r_A = y \cdot r_{\text{tetra Cu}^{2+}} + (1 - y) \cdot r_{\text{tetra Fe}^{3+}} \tag{2}$$

$$r_B = \frac{1}{2} \left\{ (0.5 - x) \cdot r_{\text{octa Li}^+} + x \cdot (x - y) \cdot r_{\text{octa Cu}^{2+}} + (1.5 - x + y) \cdot r_{\text{octa Fe}^{3+}} \right\} \tag{3}$$

In LNM series,

$$r_A = y \cdot r_{\text{tetra Mg}^{2+}} + (1 - y) \cdot r_{\text{tetra Fe}^{3+}} \tag{4}$$

$$r_B = \frac{1}{2} \left\{ (0.5 - x) \cdot r_{\text{octa Li}^+} + x \cdot (x - y) \cdot r_{\text{octa Mg}^{2+}} + (1.5 - x + y) \cdot r_{\text{octa Fe}^{3+}} \right\} \tag{5}$$

The proposed cation distributions used for the calculations of theoretical lattice constant are listed in Tables 2 and 3.
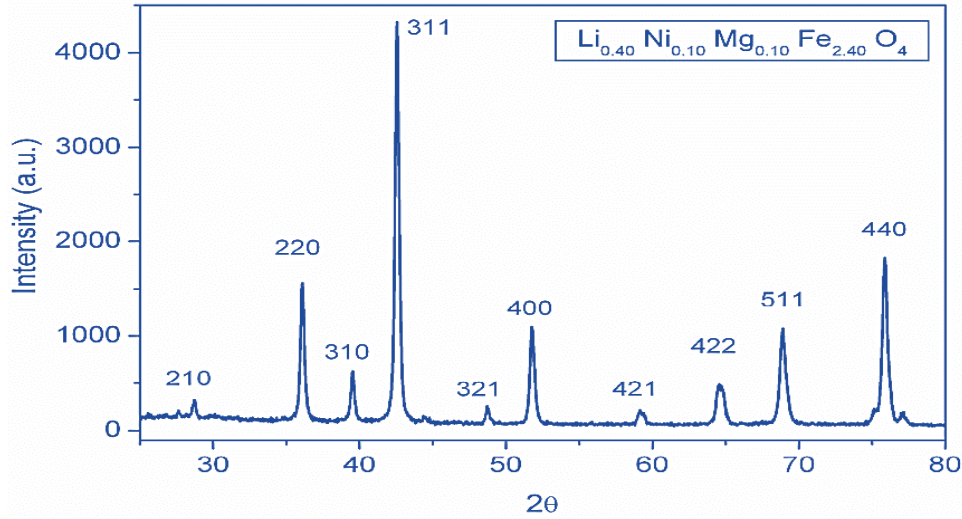
Figure 3: Typical X-ray diffraction patterns of Ni-Mg substituted (LNM, x=0.10) ferrite samples.

Tables 4 and 5 give the comparison between calculated and experimental lattice constant values. The same has been shown in the form of graph for easily depicting the trends in Figure 5 and 6 respectively.

Table 2: The proposed cation distribution for the LNC series of samples.

| $x$ | A site | B site |
|------|--------|--------|
| 0.00 | Fe | $Li_{0.5}Fe_{1.5}$ |
| 0.05 | Fe | $Li_{0.45}Ni_{0.05}Cu_{0.05}Fe_{1.45}$ |
| 0.10 | Fe | $Li_{0.4}Ni_{0.1}Cu_{0.1}Fe_{1.40}$ |
| 0.15 | $Fe_{0.985}Cu_{0.015}$ | $Li_{0.35}Ni_{0.15}Cu_{0.135}Fe_{1.365}$ |
| 0.20 | $Fe_{0.925}Cu_{0.075}$ | $Li_{0.25}Ni_{0.25}Cu_{0.175}Fe_{1.325}$ |
| 0.25 | $Fe_{0.940}Cu_{0.060}$ | $Li_{0.25}Ni_{0.25}Cu_{0.175}Fe_{1.325}$ |

The values of $r_A$ and $r_B$ can be calculated for both the systems LNC and LNM systems using the following expressions [23].

Table 3: The proposed cation distribution for the LNM series of samples

| $x$ | A site | B site |
|------|--------|--------|
| 0.00 | Fe | $Li_{0.5}Fe_{1.5}$ |
| 0.05 | Fe | $Li_{0.45}Ni_{0.05}Mg_{0.05}Fe_{1.45}$ |
| 0.10 | Fe | $Li_{0.40}Ni_{0.10}Mg_{0.10}Fe_{1.40}$ |
| 0.15 | $Fe_{0.955}Mg_{0.045}$ | $Li_{0.35}Ni_{0.15}Mg_{0.105}Fe_{1.395}$ |
| 0.20 | $Fe_{0.960}Mg_{0.040}$ | $Li_{0.30}Ni_{0.20}Mg_{0.160}Fe_{1.340}$ |
| 0.25 | $Fe_{0.975}Mg_{0.025}$ | $Li_{0.25}Ni_{0.25}Mg_{0.225}Fe_{1.275}$ |

The ionic radii of $Li^+$, $Ni^{2+}$, $Cu^{2+}$, $Mg^{2+}$, and $Fe^{3+}$ used in the calculations are taken from Shannon [24] corresponding to tetrahedral and octahedral coordination.

Table 4: Experimental and calculated lattice constants of LNC system. $Li_{0.5-x}Ni_xCu_xFe_{2.5-x}O_4$ (LNC series)

| $x$ | $a_{\text{obs}}$ | $a_{\text{cal}}$ |
|---|---|---|
| 0.00 | 8.287 | 8.3558 |
| 0.05 | 8.282 | 8.3568 |
| 0.10 | 8.298 | 8.3578 |
| 0.15 | 8.364 | 8.3589 |
| 0.20 | 8.350 | 8.3602 |
| 0.25 | 8.386 | 8.3615 |

Table 4: Experimental and calculated lattice constants of LNM system. $Li_{0.5-x}Ni_xMg_xFe_{2.5-x}O_4$ (LNM series)

| $x$ | $a_{\text{obs}}$ | $a_{\text{cal}}$ |
|---|---|---|
| 0.00 | 8.287 | 8.3558 |
| 0.05 | 8.336 | 8.3561 |
| 0.10 | 8.294 | 8.3565 |
| 0.15 | 8.364 | 8.3578 |
| 0.20 | 8.383 | 8.3581 |
| 0.25 | 8.350 | 8.3580 |

It can be clearly seen from the above figure that the trends of experimental and theoretical lattice constants for both the LNC and LNM series samples are optimally made to coincide within the limitations of experimental errors associated with the XRD technique, and thus the assigned cation distributions are reasonably accurate.
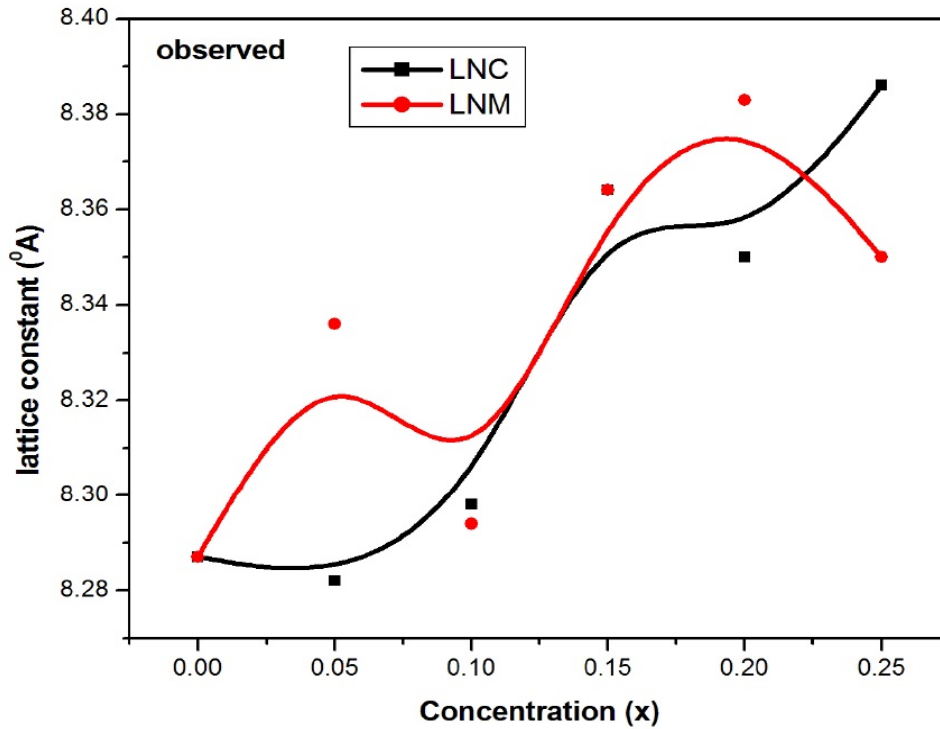


Figure 4: Variations of observed lattice constant with concentration (x) of LNC and LNM series.
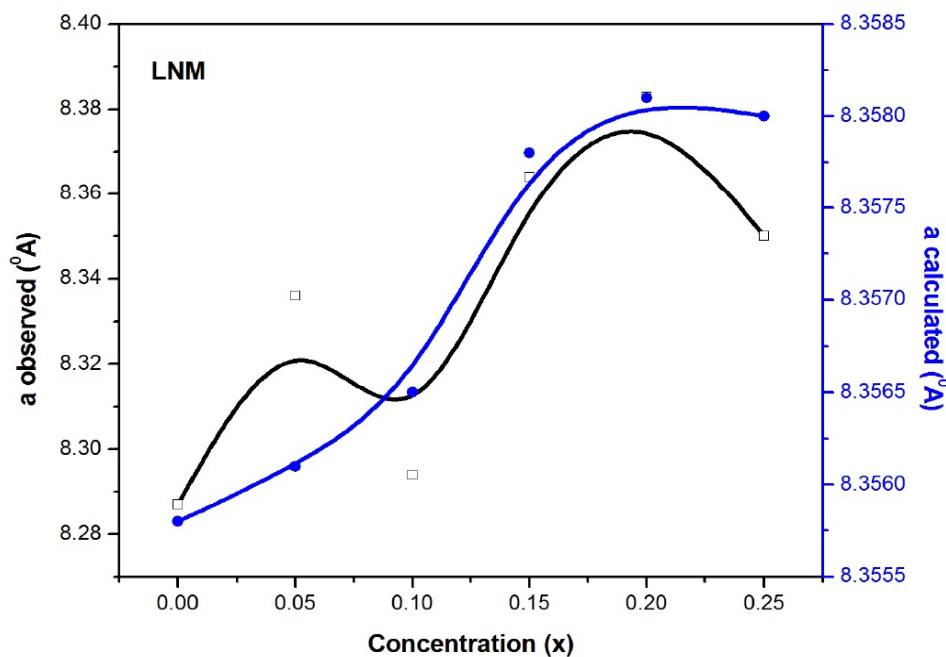
Figure 5: Comparison of variations of observed and calculated lattice constants with concentration (x) in LNM series.
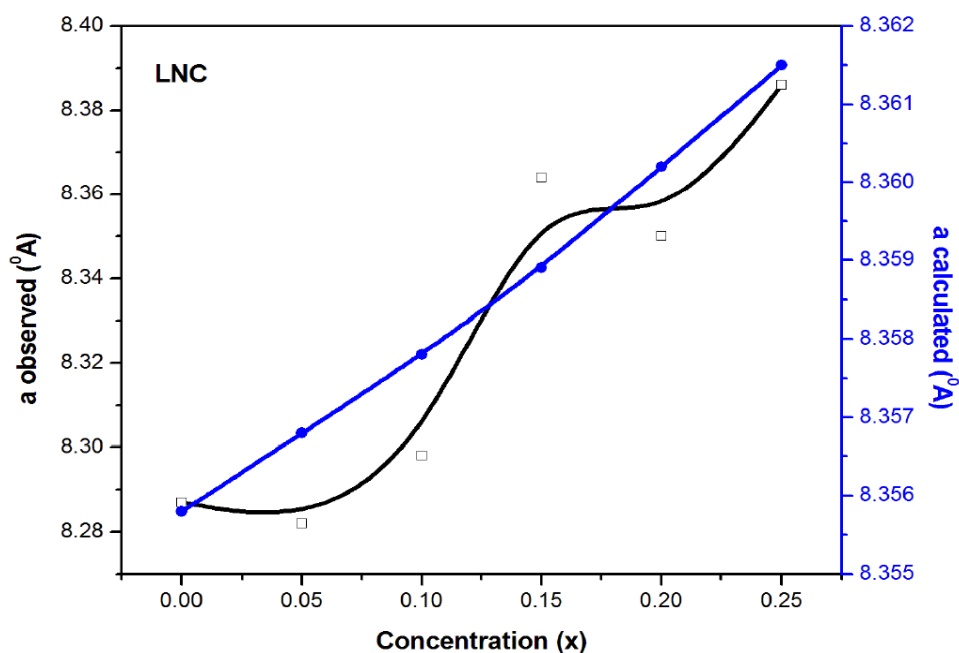


Figure 6: Comparison of variations of observed and calculated lattice constants with concentration (x) in LNC series.

## 4 Discusssion

When there is a change in the lattice constant of a crystal, it can affect the distribution of cations within the crystal lattice. The lattice constant is the distance between unit cells in a crystal lattice. Changes in lattice constant can occur due to various factors, such as temperature, pressure, or the pres-ence of impurities [25]. The distribution of cations within a crystal lattice is determined by factors like the crystal structure and the size of the cations. In an ionic crystal, cations are arranged in a specific way to achieve electrostatic stability. Here are a few possible scenarios when there is a change in lattice constant: If the lattice constant increases, the dis-tance between adjacent ions also increases. Cations

may experience a decrease in repulsion, making it more favorable for larger cations to be accommodated within the lattice. If the lattice constant decreases, the distance between adjacent ions also decreases. Smaller cations may find it more favorable to occupy the lattice sites. Significant changes in lattice constants can lead to phase transitions in the crystal structure [26]. During a phase transition, there can be a reorganization of cations in the crystal lattice to achieve a more stable arrangement at the new lattice constant. Changes in lattice constant can affect the substitution of cations in the crystal lattice. Depending on the specific conditions, different cations may be more likely to substitute for one another.

It's important to note that the behavior can vary depending on the specific crystal structure and the type of cations involved. Additionally, changes in lattice constant can be associated with changes in the material's physical and chemical properties, including its electronic, optical, and mechanical properties. Experimental studies and theoretical calculations are often used to understand these behaviors in specific materials.

The cation distribution in a material refers to the arrangement of positively charged ions (cations) within its crystal structure. This distribution can have a significant impact on the material's properties like magnetic, electronic, electric, dielectric, optical, mechanical, chemical, phase transition, and thermal conductivity, etc. [10, 27]. Understanding and controlling cation distribution is essential in the design and engineering of materials with specific desired properties for various technological applications, including electronics, catalysis, energy storage, and more. Researchers often explore different cation distributions to tailor material properties for specific functions. The cation distribution can impact phase transitions in materials. Changes in temperature or pressure may lead to structural transitions, and the distribution of cations can influence the ease and nature of these transitions. The details on the material properties other than the structural properties will be discussed in the next paper.

## 5   Conclusion

The XRD peaks 210, 211, 220, 310, 311, 321, 400, 421, 422, 511, 440 are matched well with JCPDS card (no. 38-0259). The patterns are indexed with all the planes indicative of spinel cubic crystal structure with the space group of *Fd3m*. However, the basic lithium ferrite shows some extra peaks with the hkl values of 210, 211 and 221 or 310 which are indicative of a mild phase transformation from the Fd3m space group to $P4_132$ space group. The present basic Li-ferrite sample contains a mild secondary hematite phase too apart from the major spinel crystal phase. There is a marked reduction in the magnitude of hematite phase in the XRD patterns of substituted samples when the concentration of the substituted Ni-Cu or Ni-Mg cations increases. The trends of experimental and theoretical lattice constants for both the LNC and LNM series samples are optimally made to coincide within the limitations of experimental errors associated with the XRD technique, and thus the assigned cation distributions are reasonably accurate.

## References

[1] K. C. P. V. S. K. Phanidhar Varma, B. Suryanarayana, Vemuri Raghavendra, D. Parajuli, and N. Murali. Effect of cr substitution on magnetic properties of co-cu nano ferrites. *Solid State Technology*, 63(5):8820–8827, Dec 2020. Accessed: Feb. 16, 2022. http://solidstatetechnology.us/index.php/JSST/article/view/7828

[2] R. G. Kharabe, R. S. Devan, C. M. Kanamadi, and B. K. Chougule. Dielectric properties of mixed li–ni–cd ferrites. *Smart Mater. Struct.*, 15(2):N36, Jan 2006. https://doi.org/10.1088/0964-1726/15/2/N02

[3] R. D. Sánchez, J. Rivas, P. Vaqueiro, M. A. López-Quintela, and D. Caeiro. Particle size effects on magnetic properties of yttrium iron garnets prepared by a sol–gel method. *J. Magn. Magn. Mater.*, 247(1):92–98, May 2002. https://doi.org/10.1016/S0304-8853(02)00170-1

[4] D. Parajuli, N. Murali, K. Samatha, and V. Veeraiah. Thermal, structural, morphological, functional group and first cycle charge/discharge study of co substituted lini1x-0.02mg0.02coxo2 (x = 0.00, 0.02, 0.04, 0.06, and 0.08) cathode material for libs. *AIP Adv.*, 12(8):085010, Aug 2022. https://doi.org/10.1063/5.0096297

[5] D. Parajuli, P. Taddesse, N. Murali, V. Veeraiah, and K. Samatha. Effect of zn2+ doping on thermal, structural, morphological, functional group, and electrochemical properties of layered lini0.8co0.1mn0.1o2 cathode material. *AIP Adv.*, 12(12):125012, Dec 2022. https://doi.org/10.1063/5.0122976.

[6] A. Goldman. Crystal structure of ferrites. pages 207–227, 1999. https://doi.org/10.1007/978-1-4615-4917-8_11

[7] M. M. Hessien. Synthesis and characterization of lithium ferrite by oxalate precursor

route. *J. Magn. Magn. Mater.*, 320(21):2800–2807, Nov 2008. https://doi.org/10.1016/J.JMMM.2008.06.018

[8] T. W. Mammo et al. Improved magnetic and dielectric behavior of al-cr substituted srfe12o19 nano hexaferrite. *Appl. Phys. A*, 129(12):1–10, Nov 2023. https://doi.org/10.1007/S00339-023-07157-0

[9] P. Himakar et al. Magnetic and dc electrical properties of cu doped co–zn nano-ferrites. *J. Electron. Mater.*, 50(6):3249–3257, Jun 2021. Accessed: Feb. 16, 2022. https://link.springer.com/article/10.1007/s11664-021-08760-8

[10] D. Parajuli, N. Murali, V. Raghavendra, B. Suryanarayana, K. M. Batoo, and K. Samatha. Investigation of structural, morphological and magnetic study of ni–cu-substituted li0.5fe2.5o4 ferrites. *Appl. Phys. A*, 1297(7):1–12, Jun 2023. https://doi.org/10.1007/S00339-023-06772-1

[11] D. Parajuli, N. Murali, and K. Samatha. Correlation between the magnetic and dc resistivity studies of cu substituted ni and zn in ni-zn ferrites. *BIBECHANA*, 19(1–2):61–67, Sep 2022. https://doi.org/10.3126/BIBECHANA.V19I1-2.46387

[12] E. Rezlescu, L. Sachelarie, P. D. Popa, and N. Rezlescu. Effect of substitution of divalent ions on the electrical and magnetic properties of ni-zn-me ferrites. *IEEE Trans. Magn.*, 36:3962–3967, 2000. https://doi.org/10.1109/20.914348

[13] N. Gupta, M. C. Dimri, S. C. Kashyap, and D. C. Dube. Processing and properties of cobalt-substituted lithium ferrite in the ghz frequency range. *Ceram. Int.*, 31(1):171–176, Jan 2005. https://doi.org/10.1016/J.CERAMINT.2004.04.004

[14] M. Schieber. High temperature phase transitions in lithium ferrite spinel single crystals. *J. Inorg. Nucl. Chem.*, 26(8):1363–1367, Aug 1964. https://doi.org/10.1016/0022-1902(64)80115-9

[15] N. Rezlescu, C. Doroftei, E. Rezlescu, and P. D. Popa. Lithium ferrite for gas sensing applications. *Sensors Actuators B Chem.*, 133(2):420–425, Aug 2008. https://doi.org/10.1016/J.SNB.2008.02.047

[16] B. P. Ladgaonkar, C. B. Kolekar, and A. S. Vaingankar. Infrared absorption spectroscopic study of nd3+ substituted zn-mg ferrites. *Bull. Mater. Sci.*, 25(4):351–354, 2002. https://doi.org/10.1007/BF02704131/METRICS

[17] B. Cullity. *Elements of X-ray diffraction.* Addison-Wesley Pub. Co., 1956.

[18] R. D. Shannon and C. T. Prewitt. Revised values of effective ionic radii. *Acta Crystallogr. Sect. B*, 26(7):1046–1048, Jul 1970. https://doi.org/10.1107/S0567740870003576

[19] E. W. Gorter and J. A. Schulkes. Reversal of spontaneous magnetization as a function of temperature in lifecr spinels. *Phys. Rev.*, 90(3):487, May 1953. https://doi.org/10.1103/PhysRev.90.487.2

[20] J. Smith and H. P. J. Wijn. *Ferrites.* Philips, Eindhoven, 1959.

[21] D. Ravinder, L. Balachander, and Y. C. Venudhar. Elastic behaviour of manganese substituted lithium ferrites. *Mater. Lett.*, 49(3–4):205–208, 2001. https://doi.org/10.1016/S0167-577X(00)00369-4

[22] S. A. Mazen, M. H. Abdallah, B. A. Sabrah, and H. A. M. Hashem. The effect of titanium on some physical properties of cufe2o4. *Phys. status solidi*, 134(1):263–271, Nov 1992. https://doi.org/10.1002/PSSA.2211340123

[23] S. S. Bellad, R. B. Pujar, and B. K. Chougule. Structural and magnetic properties of some mixed li-cd ferrites. *Mater. Chem. Phys.*, 52(2):166–169, Feb 1998. https://doi.org/10.1016/S0254-0584(98)80019-9

[24] R. D. Shannon and IUCr. Revised effective ionic radii and systematic studies of interatomic distances in halides and chalcogenides. *Acta Crystallogr. Sect. B*, 32(5):751–767, Sep 1976. https://doi.org/10.1107/S0567739476001551

[25] Y. B. S. B. S. Rao et al. Effect of fe doped and capping agent – structural, optical, luminescence, and antibacterial activity of zno nanoparticles. *Chem. Phys. Impact*, 7:100270, Dec 2023. https://doi.org/10.1016/J.CHPHI.2023.100270

[26] R. Wagner et al. Crystal structure of garnet-related li-ion conductor li7-3xgaxla3zr2o12: Fast li-ion conduction caused by a different cubic modification? *Chem. Mater.*, 28(6):1861–1871, Mar 2016. https://doi.org/10.1021/ACS.CHEMMATER.6B00038/SUPPL_FILE/CM6B00038_SI_005.CIF

[27] N. Murali et al. Theoretical investigation of structural, electronic, dielectric and optical characteristics of cubic perovskite baceo3. *Process. Appl. Ceram.*, 15(4):351–356, 2021. https://doi.org/10.2298/PAC2104351M